RESEARCH ARTICLE

Hubble Space Telescope Observations of Variations in Ganymede's Oxygen Atmosphere and Aurora

P. M. Molyneux[1] , J. D. Nichols[2] , N. P. Bannister[2], E. J. Bunce[2] , J. T. Clarke[3] , S. W. H. Cowley[2] , J.-C. Gérard[4] , D. Grodent[4] , S. E. Milan[2] , and C. Paty[5]

[1]Southwest Research Institute, San Antonio, TX, USA, [2]Department of Physics and Astronomy, University of Leicester, Leicester, UK, [3]Center for Space Physics, Boston University, Boston, MA, USA, [4]Laboratoire de Physique Atmosphérique et Planétaire, Université de Liège, Liège, Belgium, [5]School of Earth and Atmospheric Sciences, Georgia Institute of Technology, Atlanta, GA, USA

Abstract We present high-sensitivity Hubble Space Telescope (HST) Cosmic Origins Spectrograph and HST Space Telescope Imaging Spectrograph measurements of atmospheric OI 130.4-nm and OI] 135.6-nm emissions at Ganymede, which exhibit significant spatial and temporal variability. These observations represent the first observations of Ganymede using HST Cosmic Origins Spectrograph and of both the leading and trailing hemispheres within a single HST campaign, minimizing the potential influence of long-term changes in the Jovian plasma sheet or in Ganymede's atmosphere on the comparison of the two hemispheres. The mean disk-averaged OI] 135.6-nm/OI 130.4-nm observed intensity ratio was 2.72 ± 0.57 on the leading hemisphere and 1.42 ± 0.16 on the trailing hemisphere. The observed leading hemisphere ratios are consistent with an O_2 atmosphere, but we show that an atomic oxygen component of ~10% is required to produce the observed trailing hemisphere ratios. The excess 130.4-nm emission on the trailing hemisphere relative to that expected for an O_2 atmosphere was ~11 R. The O column density required to produce this excess is determined based on previous estimates of the electron density and temperature at Ganymede and exceeds the limit for an optically thin atmosphere. The implication that the O atmosphere is optically thick may be investigated in future by observing Ganymede as it moves into eclipse or by determining the ratio of the individual components within the 130.4-nm triplet.

1. Introduction

Ganymede's tenuous oxygen atmosphere was discovered via Hubble Space Telescope (HST) Goddard High-Resolution Spectrograph detection of the atomic oxygen emission multiplets OI 130.4 nm and OI] 135.6 nm (Hall et al., 1998). The observed double-peaked profile of the 135.6-nm feature indicated that the emissions originated from two distinct regions near Ganymede's poles. This detection, combined with the discovery of an intrinsic magnetic field at Ganymede strong enough to carve out a magnetosphere around the moon (Kivelson et al., 1996, 1997), hinted at the existence of auroral processes. Further observations using the HST Space Telescope Imaging Spectrograph (HST/STIS) confirmed that the emission was predominantly emitted from rings surrounding each pole, similar to Earth's auroral ovals (Feldman et al., 2000). Eviatar, Strobel, et al. (2001) showed that the Jovian plasma electrons near Ganymede do not possess enough energy to produce the measured OI emission intensities directly and hence must be accelerated locally within Ganymede's magnetosphere.

More recently, STIS observations of Ganymede were analyzed by McGrath et al. (2013) to determine the time-averaged locations of the auroral ovals, which were shown to lie at higher latitudes on the orbital trailing hemisphere than on the leading hemisphere. Ganymede is tidally locked to Jupiter, with the leading hemisphere facing the Earth when the satellite is at eastern elongation (phase angle 90°) and the trailing hemisphere visible from Earth at western elongation (phase angle 270°). As a result of the tidal locking, the same (trailing) hemisphere always faces upstream relative to the bulk flow of the Jovian plasma in which the satellite is embedded, which has an orbital velocity significantly larger than that of Ganymede. The difference in auroral latitude on the two hemispheres is consistent with the impinging plasma compressing the upstream (trailing hemisphere) magnetosphere towards Ganymede and stretching out the downstream (leading hemisphere) magnetosphere into a magnetotail, as predicted by magnetohydrodynamic (MHD) models (Duling et al., 2014; Jia et al., 2008, 2009; Paty & Winglee, 2004, 2006; Paty et al., 2008; Payan et al., 2015).

STIS images of Ganymede's 135.6-nm aurora have also been used by Saur et al. (2015) to constrain Ganymede's interior structure. A north-south oscillation of Ganymede's open-closed field line boundary, which corresponds to the location of the aurora (Jia et al., 2008, 2009; McGrath et al., 2013), is observed over the course of a Jovian rotation, as the offset between Jupiter's rotation and magnetic axes leads to a changing interaction between the magnetospheres of the two bodies. Saur et al. (2015) present the weak (2.0° ± 1.3°) amplitude of the observed auroral oscillation at Ganymede as evidence for a counteracting magnetic field induced in a conductive subsurface ocean, with an oscillation amplitude of 5.8° ± 1.3° predicted in the absence of an ocean.

The far ultraviolet (FUV) oxygen emissions seen at Ganymede are multiplets corresponding to the optically allowed $^3S^0$-^3P transition centered at 130.4 nm and the semiforbidden $^5S^0$-^3P transition at 135.6 nm. Both are predominantly produced by electron impact excitation of the atmosphere (Hall et al., 1998). The ratio of the intensity of the two oxygen features is dependent on the relative proportions of atomic and molecular oxygen present and on the temperature of the electrons exciting the emissions (e.g., Hall et al., 1995, 1998). For Maxwellian electron populations with temperatures between 5 and 500 eV impacting on a pure O_2 atmosphere, a ratio of ~2–3 is expected (Kanik et al., 2003). For pure O atmospheres, the expected ratio is <0.3 (Laher & Gilmore, 1990). The initial HST Goddard High-Resolution Spectrograph Ganymede spectra yielded a ratio of 1.3 ± 0.3 (Hall et al., 1998), implying a predominantly O_2 atmosphere, and HST/STIS observations revealed variations in the intensity ratio between 1.2 ± 0.2 and 3.2 ± 1.6 over a period of less than 6 hr (Feldman et al., 2000). These previous measurements of the OI] 135.6-nm/OI 130.4-nm intensity ratio were derived from observations of Ganymede's trailing hemisphere only. While the observations of Hall et al. (1998) and Feldman et al. (2000) indicated an O_2-dominated atmosphere, the relatively low signal-to-noise ratio (SNR) of the measurements rendered tentative any conclusion that there is a real temporal variation in the relative intensities of the emissions.

Here we discuss the first observations of the OI) 135.6-nm/OI 130.4-nm ratio obtained by the Cosmic Origins Spectrograph (COS), a large-aperture slitless spectrograph installed on board HST in 2009, which provides a greater than order of magnitude increase in FUV sensitivity over STIS (Green et al., 2012). We hence obtain the ratio OI] 135.6 nm/OI 130.4 nm with significantly decreased uncertainties over previous STIS observations and show that the ratio varies between the leading and trailing hemispheres, and over time. We also investigate variations in the intensities of the individual oxygen emissions between hemispheres and with System III longitude, λ_{III}, which is defined based on the configuration of Jupiter's magnetic field. The data described here represent the first observations of both orbital hemispheres within a single HST campaign, minimizing the risk of long-term changes in the Jovian plasma sheet influencing any hemispheric differences seen. Previously, the two orbital hemispheres were observed at a minimum separation of >2 years (HST campaigns 7939 and 8224). The possibility of long-term changes within the Jovian plasma, such as the decrease in density between 1998 and 2001 measured by Galileo near Europa (Bagenal et al., 2015), adds uncertainty to comparisons of observations at this timescale, and our program was designed to minimize such uncertainties as much as possible and allow a direct comparison of the leading and trailing emissions.

2. Observations

HST observations of Ganymede were obtained on 23 and 27 January and 25 February 2014 using STIS and COS. The set of observations collected on 23 January consisted of four ~890–1,410-s COS spectra of Ganymede near eastern elongation, such that the orbital leading hemisphere faced the Earth, flanked by two pairs of 885-s STIS spectral images to provide spatial context to the COS spectra. The 27 January observations were intended to follow the same sequence for the orbital trailing hemisphere with Ganymede at western elongation, but a guide star acquisition failure after the first pair of STIS exposures meant that no further data were collected on that date. The 25 February observations comprised four COS spectra and two STIS spectral images, completing the set of western elongation observations. The required rescheduling increases the possibility of plasma changes influencing our comparison of Ganymede's leading and trailing hemisphere emissions. Short-to-medium timescale effects such as increased volcanism on Io, leading to an increased plasma density, may affect the intensity of Ganymede's aurora. However, Hisaki/EXCEED observations of the 130.4-nm oxygen intensity near Io between December 2013 and April 2014, and ground-based

observations of emissions from Io's neutral sodium clouds obtained in the same period, show no significant enhancement in this time (Koga et al., 2018). A comparison of the trailing hemisphere observations obtained on 27 January and 25 February also indicates that the magnitude of Ganymede's auroral emissions was similar on both days. We therefore assume no notable variation in the plasma conditions near Ganymede during the period of our observations.

Each sequence of Ganymede observations was designed to encompass one crossing of the Jovian plasma sheet; a region near Jupiter's magnetic equator to which most of the Jovian magnetospheric plasma is confined due to the large centrifugal force experienced by the plasma as it corotates with Jupiter. The ~10° offset between Jupiter's magnetic and rotational axes leads to a varying plasma environment in the orbital plane of Ganymede over each ~10-hr System III rotational period. Ganymede crosses Jupiter's plasma sheet twice per Jovian rotation, at $\lambda_{III} = 111°$ and $\lambda_{III} = 291°$ according to the VIP4 model of Jupiter's magnetic field by Connerney et al. (1998). (The VIPAL model by Hess et al. (2011) places the plasma sheet crossings at $\lambda_{III} = 106°$ and $\lambda_{III} = 286°$. The 5° difference in the models is equivalent to an ~8-min difference in the timing of Ganymede's plasma sheet crossings, which is not large enough for the choice of model to have a significant effect on our analysis.) The timing of our observations allowed STIS observations of each of Ganymede's orbital hemispheres to be obtained at both positive and negative magnetic latitudes, θ_m, related to λ_{III} by $\theta_m = 9.5° \cos (\lambda_{III} - 201°)$ (Connerney et al., 1998), allowing the effect of the magnetic environment on the morphology and intensity of the atmospheric emissions to be studied.

COS has a primary science aperture (PSA) of 2.5". diameter. Observations were acquired using the FUV channel, which utilizes a cross delay line microchannel plate detector, and the G140L grating. All STIS spectral images were obtained using the FUV-MAMA channel, employing the G140L grating and the 52×2-arcsec slit, which has a width of 2" and a length of 25" as projected on the MAMA detector. The COS G140L dispersion is 8.03×10^{-5} nm/pixel, compared to 0.06 nm/pixel for STIS G140L, and the two instrument modes have similar plate scales (spatial resolutions) of 0.0246 arcsec/pixel (STIS G140L) and 0.023 arcsec/pixel (COS G140L along the dispersion axis; the cross-dispersion plate scale is 0.090 arcsec/pixel). Ganymede's maximum angular size was 1.70" during our observations, equivalent to a width of ~4.1 nm along the dispersion axis for STIS G140L and 5.9×10^{-3} nm for COS G140L. The 130.4- and 135.6-nm oxygen emissions and the reflected solar 133.5-nm carbon multiplet that lies between them are therefore completely separated in COS spectra of Ganymede, while in STIS spectra the three emissions overlap.

The COS spectra were reduced and extracted using CALCOS v. 2.20, providing a calibrated one-dimensional (x1d) spectral file for each observation. The x1d extraction pipeline includes a background correction performed by subtracting the averaged counts measured in two detector regions above and below the COS PSA from the extracted source spectrum. The extracted, background-corrected spectra were rebinned by five bins (0.04 nm) for improved SNR. The reflected solar component of each x1d spectrum was subtracted by scaling and fitting a Thermosphere, Ionosphere, Mesosphere, Energetics and Dynamics (TIMED)/Solar Extreme Ultraviolet Experiment (SEE) solar spectrum (Woods et al., 2000) obtained at the time of the HST observation with a time shift to account for different solar longitudes facing the Earth and Ganymede. The solar spectrum was convolved with the COS line spread function and with a Gaussian representing Ganymede's diameter to account for the extended nature of the reflection. The convolved solar spectrum was then scaled to the CII 133.5-nm feature in the x1d spectrum and subtracted from the data.

STIS spectra were extracted from the calibrated two-dimensional spectral image (x2d) files. Ganymede's position within each spectral image was determined by summing the signal at wavelengths greater than 150 nm, where the signal is dominated by reflected sunlight, in the dispersion direction. The result of the summation was a spatial profile along the slit, to which a Gaussian was fitted to locate the central pixel of Ganymede's disk in the spatial direction. A 2" (82 pixel) wide strip centered on this pixel was then extracted from the full spectral image and summed to give a spectrum. The spectrum was rebinned by four bins (0.24 nm) for improved SNR. A background correction was performed using two further 82-pixel regions located above and below Ganymede in the image, which were summed, averaged, and subtracted from the spectrum. A TIMED/SEE solar spectrum was convolved with a uniform reflecting disk of Ganymede's radius, scaled to each extracted spectrum and subtracted. Since the reflected CII 133.5-nm multiplet cannot be resolved in STIS spectra, the solar spectrum was scaled to the 140- to 145-nm region, where no significant airglow emissions are expected.

Table 1
Summary of Observations Performed in HST Campaign 13328 and Derived OI Fluxes

| HST observation ID	Identifier	Hemisphere	Instrument	Date	Start time (UTC)	Exposure time (s)[a]	OI 130.4-nm brightness[b] (R)	OI 135.6-nm brightness[b] (R)	135.6/130.4[b]	Ganymede system III longitude (°)	Ganymede phase (°)
ocbug1010	LS1	L	STIS	23 January 2014	17:08:09	885	24.5 ± 5.4	58.9 ± 5.7	2.40 ± 0.37	145.2	77.9
ocbug1020	LS2	L	STIS	23 January 2014	17:26:21	885	10.8 ± 6.3	42.4 ± 6.1	3.91 ± 1.20	155.5	78.5
lcbuh1tfq[c]	LC1	L	COS	23 January 2014	18:40:51	988		70.4 ± 1.2		198.5	81.2
lcbuh1thq[c]	LC2	L	COS	23 January 2014	18:59:14	989		74.7 ± 1.3		208.9	81.8
lcbuh1jq	LC3	L	COS	23 January 2014	20:02:29	1408 [808]	34.9 ± 1.3	74.8 ± 1.5	2.14 ± 0.06	247.0	84.2
lcbuh1tlq	LC4	L	COS	23 January 2014	20:27:42	1409	24.8 ± 0.7	66.2 ± 0.8	2.67 ± 0.05	261.3	85.0
ocbui1010	LS3	L	STIS	23 January 2014	21:53:47	885	33.7 ± 7.6	82.5 ± 8.4	2.45 ± 0.38	307.9	87.9
ocbui1020	LS4	L	STIS	23 January 2014	22:11:57	885	48.0 ± 7.8	129.6 ± 8.8	2.70 ± 0.29	318.2	88.5
ocbug2010	TS1	T	STIS	27 January 2014	12:00:37	885	31.3 ± 8.9	50.6 ± 7.9	1.62 ± 0.41	10.4	269.2
ocbug2020	TS2	T	STIS	27 January 2014	12:18:48	885	35.1 ± 9.2	41.8 ± 8.2	1.19 ± 0.36	20.8	269.9
lcbug3f0q	TC1	T	COS	25 February 2014	01:22:37	988 [688]	25.2 ± 1.7	36.7 ± 1.5	1.46 ± 0.09	32.4	268.2
lcbug3f3q	TC2	T	COS	25 February 2014	01:40:57	989	29.6 ± 1.2	45.3 ± 1.1	1.53 ± 0.06	42.9	268.9
lcbug3f7q[d]	TC3	T	COS	25 February 2014	02:43:42	1408 [508]	67.1 ± 2.9	36.9 ± 2.0	0.55 ± 0.06	80.6	271.2
lcbug3f9q	TC4	T	COS	25 February 2014	03:08:52	1409	22.5 ± 0.8	31.0 ± 0.7	1.38 ± 0.05	94.9	272.0
ocbuh3010	TS3	T	STIS	25 February 2014	04:34:59	885	32.5 ± 7.4	39.0 ± 5.7	1.20 ± 0.30	141.5	274.9
ocbuh3020	TS4	T	STIS	25 February 2014	04:53:10	885	19.4 ± 6.5	30.9 ± 5.7	1.59 ± 0.49	151.8	275.5

Note. HST = Hubble Space Telescope.
[a] For exposures contaminated with geocoronal 130.4-nm emissions, the auroral intensities were extracted from the uncontaminated portion of the exposure, shown in square brackets. [b] Disk-averaged values. Errors represent 1σ statistical uncertainties due to detector counting statistics (e.g., Poisson noise). [c] The 130.4-nm emissions were not measured for exposures lcbuh1tfq and lcbuh1thq (LC1 and LC2) as they fell outside of the active detector area. [d] The 130.4-nm emissions in observation TC3 remained elevated after removal of the most highly contaminated part of the exposure. This observation was excluded from further analysis.

Disk-averaged 135.6- and 130.4-nm intensities were calculated from the COS and STIS spectra by summing the signal over all pixels within the $2'' \times 2''$ extraction region centered at those wavelengths for STIS, and within the 2.5" PSA for COS, and normalizing to the projected size of Ganymede's disk in pixels. Previous observations of Ganymede have shown that a significant fraction of the aurora can be located outside of the disk (Feldman et al., 2000; McGrath et al., 2013; Musacchio et al., 2017; Saur et al., 2015), and including counts from the wider instrument aperture rather than only those originating within the disk is therefore important. Ganymede's angular size during our observations was between 1.59 and 1.70" The STIS-derived disk averages therefore included counts out to 1.18–1.25 R_G from Ganymede's center, where R_G is the radius of Ganymede. For COS, the aperture covered the region out to 1.47–1.56 R_G, but in practice the throughput decreases outside of the central ~1.4" (Green et al., 2012). Our COS disk-averaged intensities may therefore be underestimated to an extent that depends on the exact locations of the emissions, which are known to be highly variable (e.g., Feldman et al., 2000), and is therefore difficult to quantify. Since the throughput fall off applies at all wavelengths, OI] 135.6-nm/OI 130.4-nm ratios derived from COS disk averages remain accurate.

STIS images of Ganymede's 135.6- and 130.4-nm aurora were extracted from the flat-fielded (flt) image files, to allow for any change in sensitivity across the 2" slit width. Pairs of images taken consecutively were summed for improved SNR. Again, background noise was evaluated above and below the extracted region, averaged and subtracted from the data. The reflected solar background was corrected for by modeling Lambertian reflection from a uniform disk with an albedo as determined from the TIMED/SEE fit to the 133.5-nm feature in the COS spectra. We measured a mean albedo of 1.5 ± 0.3% on the leading hemisphere and 2.2 ± 0.3% on the trailing.

Table 1 summarizes the timing and geometry of the observations and gives the disk-averaged 130.4- and 135.6-nm intensity in Rayleighs (1 $R = \frac{10^6}{4\pi}$ photons·s^{-1}·cm^{-2}·sr^{-1}) observed in each case, after subtraction of reflected sunlight. Also shown are disk-averaged OI] 135.6-nm/OI 130.4-nm emission ratios calculated from these values. Each observation is assigned an identifier indicating the instrument used, the hemisphere observed, and the position of that observation within the observing sequence: for example, "TC1" denotes the first observation of the trailing hemisphere using COS.

Figure 1 shows representative COS emission spectra in the region 129–138 nm for Ganymede's leading (Figures 1a and 1b) and trailing (Figures 1c and 1d) hemispheres, before and after subtraction of a fitted TIMED/SEE solar spectrum. The spectra shown were extracted from observations LC3 and TC2. A STIS spectrum (observation LS1) superposed with a scaled solar spectrum is shown in Figure 1e to illustrate the difference in response of the two instruments. STIS images of Ganymede's 135.6- and 130.4-nm emissions are shown in Figure 2, alongside diagrams illustrating the orbital phase of Ganymede and its position relative to the Jovian
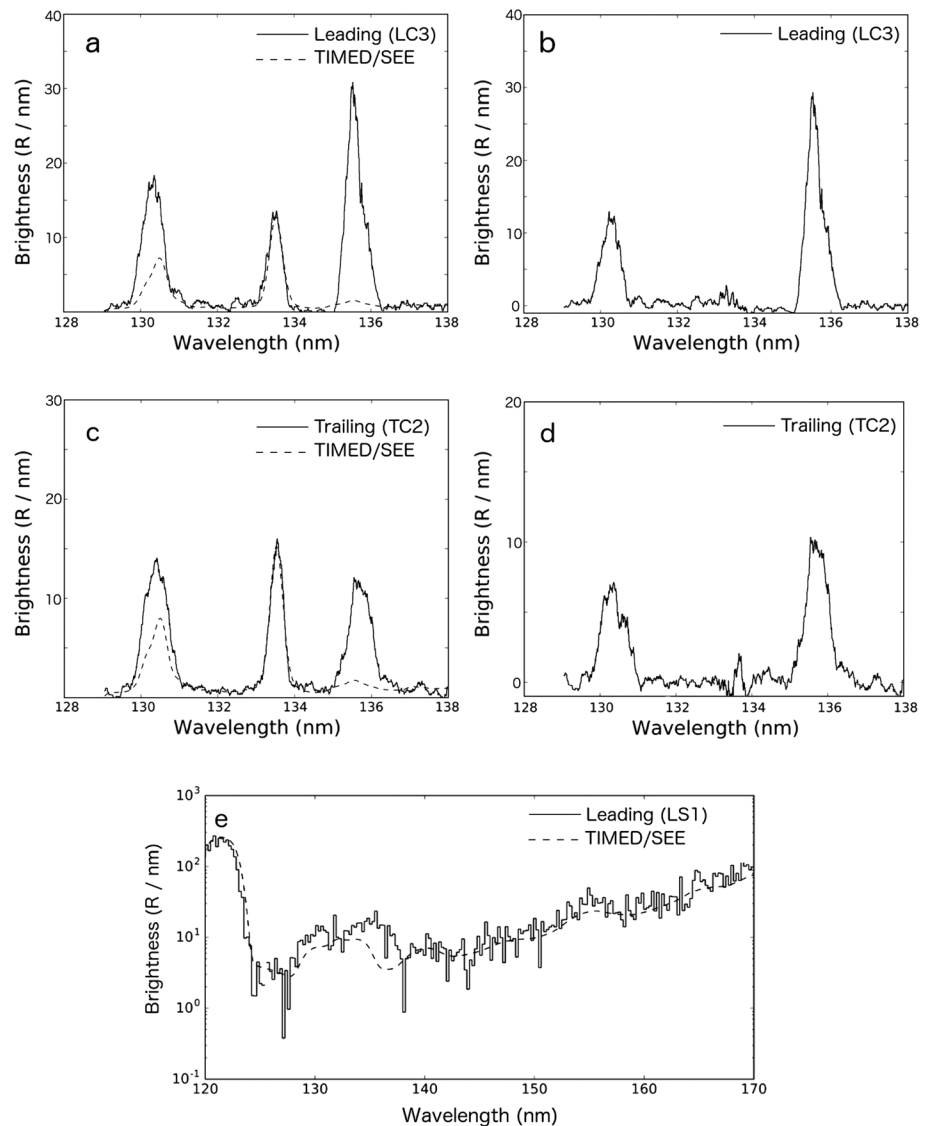
Figure 1. Overview of COS observations of Ganymede's aurora. (a–d) The 129- to 138-nm COS spectra of Ganymede's leading (a, b) and trailing (c, d) hemispheres in which the oxygen emissions at 130.4 and 135.6 nm are clearly visible (also visible is reflected solar C II at 133.5 nm). Spectra extracted from observations LC3 and TC2 are shown before (a, c) and after (b, d) subtraction of a fitted TIMED/SEE solar spectrum (dashed line). All spectra are smoothed to 25-pixel (0.2 nm) resolution for display purposes. (e) STIS spectrum from observation LS1 (solid line), rebinned to 4 pixel (0.24 nm) resolution. A fitted TIMED/SEE spectrum convolved with a uniform reflecting disk of Ganymede radius is shown as a dashed line. TIMED/SEE = Thermosphere, Ionosphere, Mesosphere, Energetics and Dynamics/Solar Extreme Ultraviolet Experiment; COS = Cosmic Origins Spectrograph.

plasma sheet during each observation. Also shown are color ratio images showing the variation of the 135.6-/130.4-nm ratio over Ganymede's disk. All images have been rotated to point Jovian north upward.

During observations LC1 and LC2 the 130.4-nm multiplet lay outside of the active detector area. These observations therefore cannot be used to determine the oxygen emission ratio and are included in analysis of the 135.6-nm emissions only. Two further COS exposures (LC3 and TC3) showed greatly increased 130.4-nm flux relative to the other observations, indicating contamination by geocoronal airglow. We used TIMETAG data to split these observations into ~300-s subexposures and compared the 130.4-nm intensity to that in the uncontaminated observations in order to identify any portions of LC3 and TC3 that were suitable for further analysis. The 130.4-nm emission intensity in both exposures decreased over time, stabilizing during the last 808 s of LC3 and the last 508 s of TC3. The measured 130.4-nm intensity for the stable portion of LC3 (62 R) was
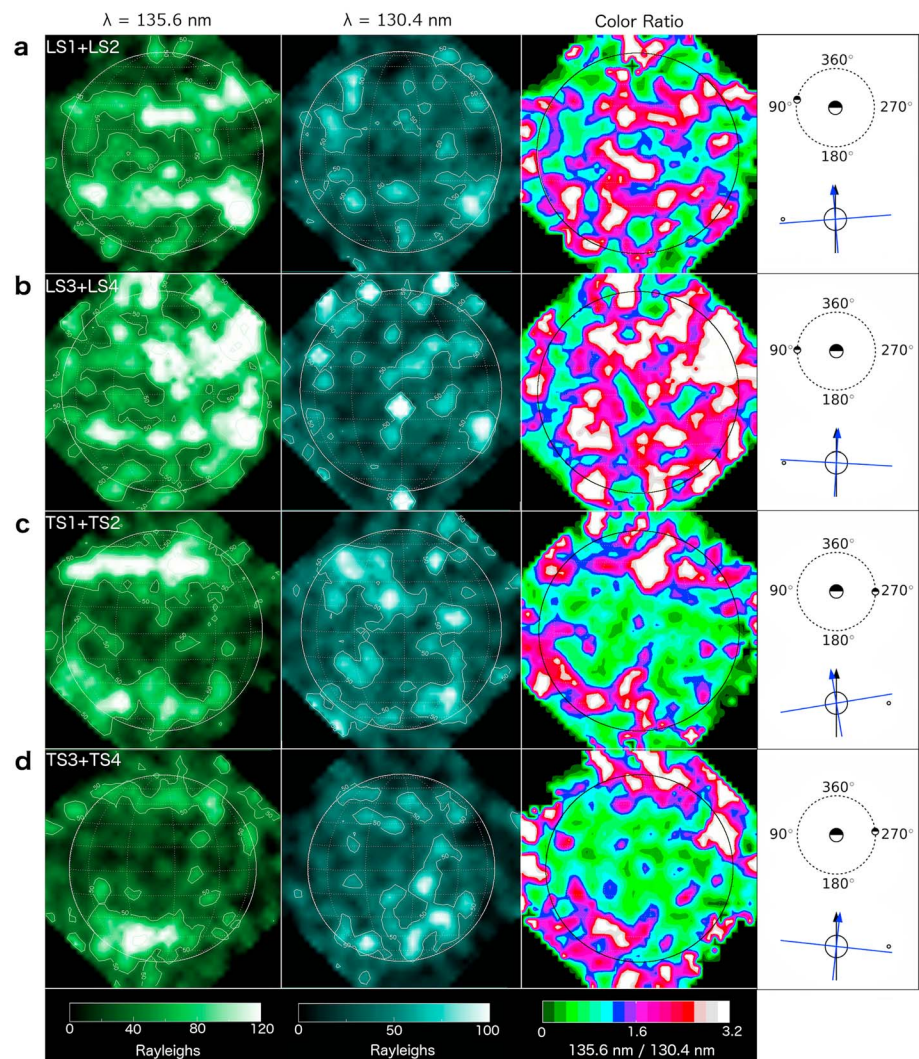
Figure 2. Space Telescope Imaging Spectrograph 135.6 nm (left column), 130.4 nm (middle column), and color ratio (right column) images of Ganymede's leading (a, b) and trailing (c, d) hemispheres. To improve signal-to-noise, each panel is the sum of two consecutive 885-s images. Images have been resampled and smoothed for display. Corresponding diagrams indicating Ganymede's orbital phase and position relative to the Jovian plasma sheet are also shown. All images are rotated to point Jovian north upward.

within one standard deviation of the mean intensity measured for the other COS exposures (mean 67 R; standard deviation 15 R—these values are higher than those shown in Table 1 as they include the reflected sunlight component), but for TC3 the emissions remained elevated relative to the other observations, at 102 R. We therefore included 808 s of observation LC3 in our analysis of Ganymede's oxygen atmosphere but excluded TC3 as we could not be confident that the geocoronal emission was completely removed. A similar consideration of the less contaminated exposures revealed that the first 300 s of TC1 contained elevated 130.4-nm emissions (125 R), and we therefore also excluded this portion of the exposure from the analysis.

3. Results

3.1. Measured Auroral Brightness and OI Emission Ratios

Similar to previous analysis of Ganymede's FUV aurora by Feldman et al. (2000), we observe large variations in both the intensity of the individual OI emissions and in the ratio of the two over the ~5-hr timescale of each observation sequence. The magnitude of the ratio on the leading hemisphere was consistently higher than

that on the trailing hemisphere for our observations: COS ratios ranged from 2.14 ± 0.06 to 2.67 ± 0.05 on the leading hemisphere and from 1.38 ± 0.05 to 1.53 ± 0.06 on the trailing hemisphere. STIS spectra yielded similar ranges of 2.41 ± 0.37 to 3.93 ± 1.20 for the leading hemisphere and 1.19 ± 0.36 to 1.61 ± 0.41 for the trailing hemisphere. The mean ratios (plus-minus standard deviation) taking all STIS and COS spectra into account were 2.72 ± 0.57 and 1.42 ± 0.16 for the leading and trailing hemispheres, respectively.

The 135.6-nm emission was consistently brighter on the leading hemisphere: the mean brightness (plus-minus standard deviation) there was 75 ± 24 R, compared to 39 ± 7 R on the trailing hemisphere. The 130.4-nm emission, however, was of a similar brightness on the two hemispheres, with a mean intensity of 30 ± 12 R on the leading hemisphere and 28 ± 5 R on the trailing hemisphere. The measured standard deviations indicate that there was more temporal variation in the intensities of both OI emissions on the leading hemisphere.

### 3.2. Auroral Variations With System III Longitude

STIS images of each hemisphere were obtained when the moon was both north (magnetic latitudes $\theta_m > 0°$) and south ($\theta_m < 0°$) of the Jovian plasma sheet equator. In this section we investigate the relationship between the disk-averaged auroral intensity at Ganymede and the moon's position relative to the plasma sheet and briefly summarize potential trends in the auroral morphology, as observed by STIS. We focus mainly on the 135.6-nm emissions as the higher solar flux and risk of geocoronal contamination at 130.4 nm lead to larger uncertainties for the 130.4 nm aurora but include a brief discussion of the 130.4 nm morphology in section 3.2.2.

3.2.1. Disk-Averaged Intensity

Figure 3 shows the brightness of Ganymede's 135.6-nm emissions as a function of λ_{III}. Intensities extracted from previous HST data sets (campaigns 7939, 8224, and 12244: see Feldman et al., 2000; McGrath et al., 2013; Musacchio et al., 2017; Saur et al., 2015, for descriptions of the data sets) are also included as faded points to extend the range of longitudes covered and indicate how our data compare to previous observations. The shaded areas in Figure 2 indicate the regions of densest Jovian plasma, at $|\theta_m| < 5°$. Our brightest leading hemisphere observations were obtained within one of these regions just after the $\lambda_{III} = 291°$ plasma sheet crossing ($\theta_m = -2.8°, -4.4°$). In contrast, the average intensity of the trailing hemisphere emissions within the densest region was slightly lower than the average intensity at $|\theta_m| > 5°$. We measured a mean 135.6 nm intensity (plus-minus standard deviation) of 36 ± 4 R on the trailing hemisphere while Ganymede was within this region, compared to 41 ± 7 R outside of it. While observations are sparse and the standard deviation is relatively large, Musacchio et al. (2017) also note this difference in the behavior of the two hemispheres near the plasma sheet center in their analysis of the morphology of Ganymede's aurora as observed in previous HST/STIS campaigns. We used the TIMETAG data to split the trailing hemisphere COS exposure closest to $\lambda_{III} = 111°$ (TC4) into seven 200-s portions to look for evidence of a systematic change in auroral intensity as Ganymede moved closer to the magnetic equator over the course of the observation. The resulting 135.6-nm intensities are shown as an inset in Figure 3c. While there appears to be some variation in the intensity over this time, there is no evidence of a statistically significant relationship between intensity and λ_{III}.

Based on Figure 3, we noted that, with the exception of exposure LS4, our observations are dimmer than previous observations obtained at similar λ_{III}. All brightness values were extracted using the same procedure, and the intensities we measured for the previous HST campaigns agree with previously published intensities (Feldman et al., 2000; Musacchio et al., 2017) within the statistical uncertainties (small differences from the published values may be due to slight variations in the data reduction process, particularly the solar subtraction and the choice of detector regions used to estimate the background noise).

Table 2 shows the mean brightness of Ganymede's 135.6-nm emissions during HST campaigns 7939, 8224, and 12244 and the ratio of the previously observed 135.6-nm brightness values to those measured during our more recent campaign (13328). Separate mean brightness values were calculated for observations at $|\theta_m| > 5°$ and $|\theta_m| < 5°$ to allow for the effect of expected plasma density variations with magnetic latitude. We find that Ganymede's 135.6-nm trailing hemisphere aurora was on average a factor of 1.50 ± 0.18 ($|\theta_m| > 5°$) to 1.53 ± 0.18 ($|\theta_m| < 5°$) brighter in HST campaign 7939 (obtained in 1998) than in the 2014 observations. The leading hemisphere was last observed in 2010 and 2011 (HST campaign 12244), in two
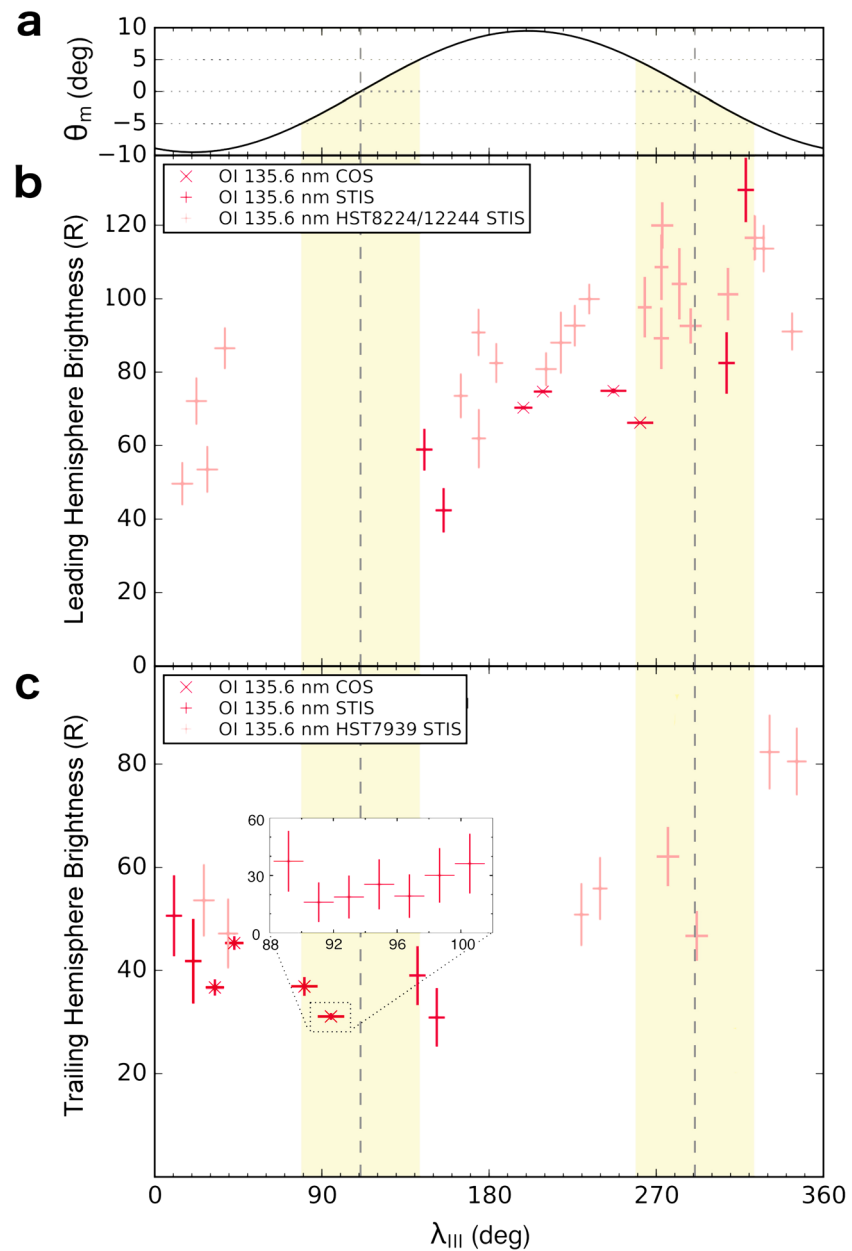
Figure 3. (a) Magnetic latitude (θ_m) of Ganymede versus System III longitude (λ_{III}). (b) Brightness (Rayleighs) of Ganymede's leading hemisphere 135.6-nm emissions versus λ_{III}. (c) Brightness (Rayleighs) of Ganymede's trailing hemisphere 135.6-nm emissions versus λ_{III}. The faded points are extracted from previous HST/STIS observations of Ganymede: program IDs are shown in the figure legends. The vertical shaded regions indicate when Ganymede is within the regions of densest Jovian plasma, at $|\theta_m| < 5°$. The inset in panel (c) shows the 135.6-nm intensity in seven 200-s subexposures extracted from observation TC4 (see text). HST = Hubble Space Telescope; COS = Cosmic Origins Spectrograph; STIS = Space Telescope Imaging Spectrograph.

visits separated by ~11 months. The mean auroral intensity measured for $|\theta_m| > 5°$ was brighter than the leading hemisphere intensities observed in 2014 by a factor of 1.41 ± 0.14 during the first of these visits, but this decreased to 1.07 ± 0.13 by the second visit. At $|\theta_m| < 5°$ the ratio also decreased between the two visits of campaign 12244, but the mean leading hemisphere intensity measured during campaign 13328 at low magnetic latitudes is heavily influenced by observation LS4, in which the 135.6-nm emissions were ~70% brighter than the mean value measured from the other observations. The ratio of auroral brightness measured in previous campaigns to that measured in 2014 for the leading hemisphere at $|\theta_m| < 5°$ may

Table 2
Mean 135.6-nm Auroral Intensities at Ganymede as Measured in Previous HST Campaigns, and Their Ratio to the Intensities Measured in the 2014 Observations

HST campaign	Date	Hemisphere	135.6-nm intensity (R)[a,b]		Ratio to HST 13328 intensity[b]	
			$\|\theta_m\| < 5°$	$\|\theta_m\| > 5°$	$\|\theta_m\| < 5°$	$\|\theta_m\| > 5°$
8224	23 December 2000	L	106.0 ± 3.6		1.14 ± 0.20 [1.43 ± 0.12]	
12244	19 November 2010	L	106.3 ± 9.7	90.5 ± 4.3	1.15 ± 0.22 [1.43 ± 0.17]	1.41 ± 0.14
12244	01 October 2011	L	96.6 ± 5.2	68.7 ± 6.2	1.04 ± 0.18 [1.30 ± 0.12]	1.07 ± 0.13
13328	23 January 2014	L	92.8 ± 15.5 [74.3 ± 5.8]	64.3 ± 5.5		
7939	30 October 1998	T	54.4 ± 5.4	61.7 ± 5.8	1.53 ± 0.18	1.50 ± 0.18
13328	27 January 2014, 25 February 2014	T	35.6 ± 2.3	41.1 ± 3.0		

Note. HST = Hubble Space Telescope.
[a]Uncertainties represent standard error on the mean values.   [b]Values in square brackets were calculated with observation LS4 excluded (see text).

therefore be underestimated if brightening events like this are not typical. To indicate the influence of observation LS4, brightness ratios calculated with this measurement excluded are also shown in Table 2.

The reduced intensity of the 2014 observations compared to the previous STIS observations suggests a long-term change either in Ganymede's atmosphere or in the Jovian plasma that excites the emissions. Roth et al. (2016) describe a similar reduction in auroral brightness at Europa, with the 135.6-nm aurora appearing ~50% brighter during 1999 than in 2012–2015. The observation of reduced auroral emissions at both moons during the same period suggests that the effect may be related to a long-term decrease in the Jovian plasma density rather than processes local to Ganymede.

3.2.2. Morphology

For all STIS 135.6-nm images, we observed brighter aurora in the polar region closer to the plasma sheet equator. The north/south intensity ratios for the leading and trailing observations north of the magnetic equator (LS1, LS2: θ_m = 5.4°, 6.7°, Figure 2a; TS3, TS4: θ_m = 4.9°, 6.2°, Figure 2d) were 0.88 ± 0.01 and 0.83 ± 0.02, respectively. The north/south ratios for observations below the plasma sheet equator (LS3, LS4: θ_m = −2.8°, −4.4°, Figure 2b; TS1, TS2: θ_m = −9.3°, −9.5°, Figure 2c) were 1.32 ± 0.02 for the leading hemisphere and 1.20 ± 0.01 for the trailing hemisphere. Most of the variation was observed in the northern aurora. At negative magnetic latitudes the intensity of the 135.6-nm northern leading hemisphere aurora increased by 71%, and the northern trailing hemisphere aurora intensity increased by 46% relative to the intensities observed at $\theta_m > 0°$. The southern aurora varied by <1% in the trailing hemisphere 135.6-nm images and by 14% on the leading hemisphere. Both northern and southern aurora were brighter at $\theta_m < 0°$ on both of Ganymede's orbital hemispheres.

The 130.4-nm images are noisier than the 135.6-nm images and have less well-defined aurora but follow the same general trend of more variation in the northern hemisphere and less in the southern. Similar to the 135.6-nm aurora, the 130.4-nm emissions were brighter for $\theta_m < 0°$ on both orbital hemispheres. The northern (southern) emissions were 14% (5%) brighter on the leading hemisphere and 40% (10%) brighter on the trailing hemisphere at $\theta_m < 0°$ relative to the values measured at $\theta_m > 0°$.

The leading hemisphere 135.6-nm images obtained when Ganymede was below the plasma sheet equator (LS3, LS4; θ_m = −2.8°, −4.4°) contained the brightest auroral emissions of all of our observations. From Table 1 and Figure 3 we see that the disk-averaged auroral intensities were particularly high for LS4. A comparison of the individual STIS exposures used to produce Figure 2b indicates that both the southern and northern 135.6-nm aurora increased in intensity in LS4, by ~10% and ~20%, respectively. The largest increase in intensity was observed in the northern Jupiter-facing quadrant of the image (e.g., upper right in Figure 2b), which was 27% brighter in LS4. Some brightening was also observed in the 130.4-nm aurora, but the Jupiter-facing quadrant intensity increased by just 10%, and there was not a clear correlation between the 135.6- and 130.4-nm morphology in this quadrant. It is therefore difficult to attribute the brightening to a specific process such as temporarily increased n_e, which would affect both emissions proportionally.

Auroral brightening in the polar hemisphere closest to the magnetic equator has previously been observed at Io and Europa (Retherford et al., 2003; Roth et al., 2016) and is attributed to the majority of the Jovian magnetospheric electron population being located above the brighter hemisphere (Retherford et al., 2003). Our
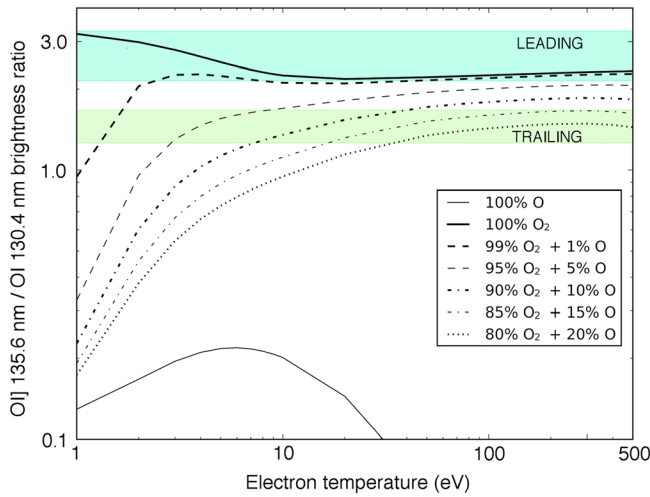
Figure 4. Expected OI] 135.6-nm/OI 130.4-nm emission ratios for electron impact excitation of atmospheres with various proportions of O and O_2 (shown in legend). The shaded areas indicate the observed mean ratio ±1 standard deviation for Ganymede's two orbital hemispheres. Resonant scattering of 130.4 nm was not included in this model (see text).

observations are consistent with this explanation, although we note that Musacchio et al. (2017) observed generally brighter emissions in the southern hemisphere aurora than the northern hemisphere at all magnetic latitudes, indicating that at Ganymede the interaction is potentially complicated by the presence of the magnetosphere.
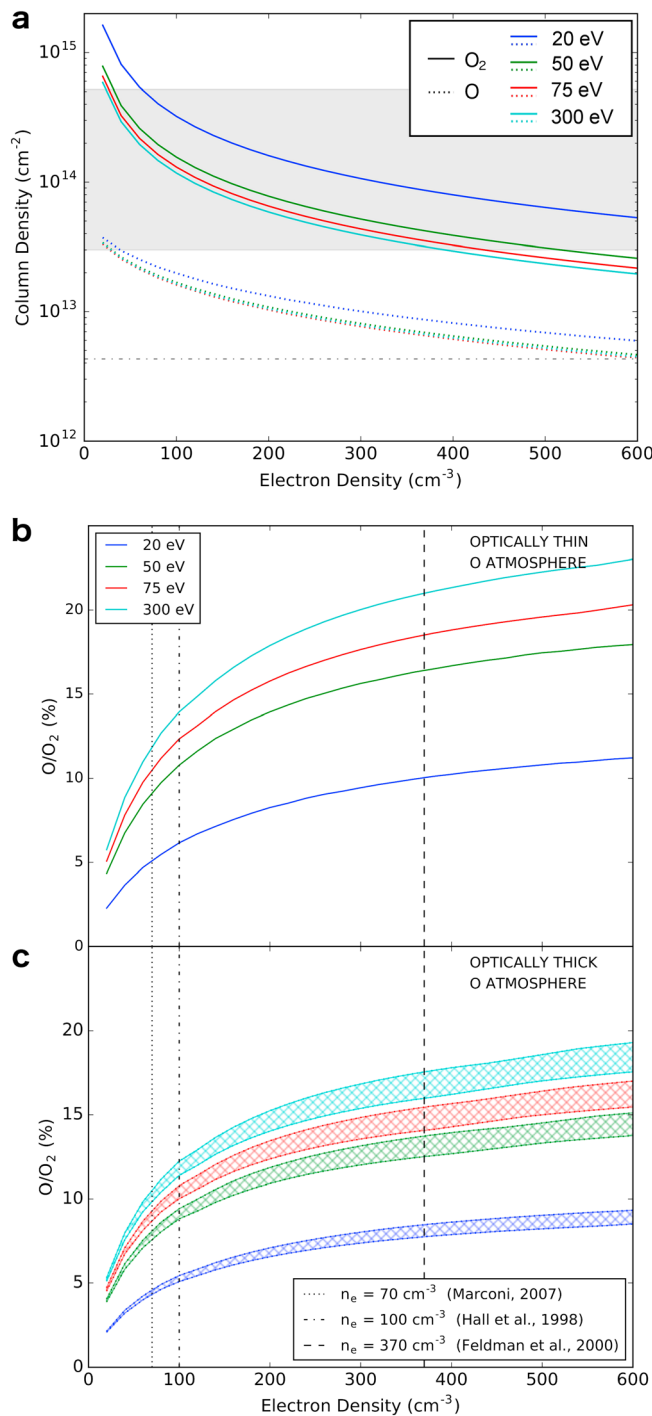
4. Discussion

4.1. Variations in the OI Emission Ratio

4.1.1. Disk-Averaged Atmosphere

Our observations show considerable variation in the OI] 135.6-nm/OI 130.4-nm intensity ratio in Ganymede's atmosphere, both temporally and between hemispheres. The OI emissions observed at Ganymede are produced predominantly through electron impact dissociative excitation of molecular oxygen. The brightness in Rayleighs of each emission excited through this process can be estimated as follows (Hall et al., 1995):

$$B_\lambda = \frac{n_e N[O_2] C_\lambda}{10^6},$$
(1)

where n_e is the electron density, $N[O_2]$ is the disk-averaged O_2 column density, and C_λ is the rate coefficient for emission at wavelength λ, which is dependent on electron temperature T_e. Therefore, the expected OI] 135.6-nm/OI 130.4-nm intensity ratio for electron impact dissociative excitation of a pure O_2 atmosphere is equivalent to the ratio of the 135.6- and 130.4-nm emission rate coefficients. Kanik et al. (2003) derived this ratio using experimentally measured cross sections for O_2 dissociation by electrons with T_e up to 600 eV and obtained values >2. Smaller emission ratios, as observed on Ganymede's trailing hemisphere, imply a contribution from electron impact excitation of atomic oxygen. The brightness of the 135.6- and 130.4-nm emissions due to this process can similarly be calculated using equation (1) with appropriate rate coefficients and with the disk-averaged O column density, $N[O]$, in place of $N[O_2]$. Hence, we can estimate the O/O_2 mixing ratio at Ganymede based on the observed OI emission ratio.

Figure 4 shows the expected OI intensity ratio for Maxwellian electron populations with T_e up to 500 eV impacting atmospheres with a range of O/O_2 ratios. The plotted values are based on experimentally determined cross sections for electron impact excitation of O (Laher & Gilmore, 1990) and dissociative excitation of O_2 (Kanik et al., 2003). Our leading hemisphere ratios are consistent with an atmosphere with $O/O_2 < 1\%$, but the ratios we measured on the trailing hemisphere require the presence of a substantial atomic oxygen component for electron temperatures above a few eV. Analysis of previous STIS observations of Ganymede by Eviatar, Strobel, et al. (2001) indicates that the auroral emissions are excited by a Maxwellian electron distribution with temperature in the range 75–300 eV. If we consider the auroral emissions to be entirely due to electron impact excitation of O and O_2, our observed ratios therefore imply that atomic oxygen comprises >10% of the trailing hemisphere atmosphere. However, as the atmospheric O density increases, the contribution of resonant scattering of sunlight to the 130.4-nm emission intensity becomes increasingly important, and atmospheric mixing ratios derived from electron impact excitation rates alone may therefore overestimate the amount of O present. To account for this, we performed a more detailed analysis of the relative contributions of each excitation process.

For the mean trailing hemisphere 135.6-nm intensity of 39 R, the 130.4-nm intensity required to achieve the OI] 135.6-nm/OI 130.4-nm intensity ratio of ~2.3 determined by Kanik et al. (2003) for dissociative excitation of O_2 is 17 R. The mean trailing hemisphere 130.4-nm emission intensity was 28 R, leaving an excess of 11 R to be explained by resonance scattering and electron impact excitation of atomic oxygen. We calculated the O column density required to produce this excess by combining equation (1) with an approximation for solar resonance scattering given by Hall et al. (1995, 1998) to give

$$N[O] = 10^6 B_\lambda \left[n_e C_\lambda + g \left[\frac{\omega(\tau)}{\tau} \right] \right]^{-1}.$$
(2)

Figure 5. (a) Estimated column densities of O and O_2 at Ganymede based on observed trailing hemisphere 130.4- and 135.6-nm emissions for a range of electron densities and temperatures. The shaded region shows the range of O_2 column densities inferred from previous observations of Ganymede. The dashed horizontal line at 4.3×10^{12} cm^{-2} indicates the maximum column density for an optically thin O atmosphere at a temperature of 150 K. (b) O/O_2 mixing ratios derived from the estimated column densities of O and O_2 at Ganymede shown in (a). (c) As in (b) but with O column densities calculated using electron impact excitation rates corrected to account for cascade and radiative trapping effects in an optically thick atmosphere. The width of the curves accounts for excitation rate correction factors in the range 1.245 to 1.40 (Cotton et al., 1993).

Here g is the resonance scattering probability or g-factor (Barth, 1969), which is dependent on the solar flux at Ganymede, τ is the line-center optical depth, and $\omega(\tau)$ is the effective resonant scattering albedo. All other quantities are as defined for equation (1). We used values for $\omega(\tau)$ derived by Lee and Meier (1980) and calculated a g-factor of 4.96×10^{-7} s^{-1} using the 130.4-nm solar flux measured by TIMED/SEE scaled to 5.2 AU. The plasma properties at Ganymede are not well characterized, so the calculation was performed for $n_e = 20$–600 cm^{-3} and $T_e = 20, 50, 75,$ and 300 eV. We then calculated O_2 column densities based on the mean trailing hemisphere 135.6 nm emission intensity of 39 R using equation (1). Finally, we derived O/O_2 mixing ratios from the calculated O and O_2 column densities.

Figure 5a shows the O and O_2 column densities required to produce the observed trailing hemisphere emission intensities as a function of n_e and T_e. The O/O_2 mixing ratio corresponding to these column densities is shown in Figure 5b. Feldman et al. (2000) estimated an O_2 column density at Ganymede in the range 0.3–5.2×10^{14} cm^{-2}, where the upper limit is the O_2 abundance limit derived by Broadfoot et al. (1981) from a Voyager ultraviolet spectrometer stellar occultation measurement. This range is shown as a shaded region in Figure 5a and is in good agreement with the range of O_2 column densities we calculated. Also plotted is a horizontal line indicating the maximum column density for an optically thin O atmosphere (e.g., the column density for optical depth $\tau_{O\_130.4} = 1$), which we calculated as 4.3×10^{12} cm^{-2} for a temperature of 150 K and an oscillator strength $f = 0.047$ (Stone & Zipf, 1974). The O column densities we calculated ranged from 4.4×10^{12} cm^{-2} for $n_e = 600$ cm^{-3} and $T_e = 75$ eV to 3.7×10^{13} cm^{-2} for $n_e = 20$ cm^{-3} and $T_e = 20$ eV.

The O column densities we calculated are larger than the optically thin limit, only approaching optically thin values at the highest electron densities considered. This has implications for the derived O/O_2 mixing ratio, since the published cross sections for electron impact on O apply to optically thin conditions. For optically thick atmospheres, the 130.4-nm cross sections are enhanced due to cascade and radiative trapping effects, reducing the mixing ratio required to explain the 11 R excess. Models by Cotton et al. (1993) suggest a cross section enhancement factor of ~1.245 to 1.40. Figure 5c shows the range of O/O_2 ratios that could support the 11 R 130.4-nm excess at Ganymede if the O atmosphere is optically thick, based on these enhancement factors. The vertical lines in Figures 5b and 5c show values of n_e that have been adopted in previous studies of Ganymede's atmosphere (Eviatar, Strobel, et al., 2001; Feldman et al., 2000; Marconi, 2007). All three values were derived from measurements taken during the Galileo G1 and G2 flybys of Ganymede (Gurnett et al., 1996; Eviatar, Vasyliūnas, et al., 2001).

At low n_e and T_e, the observed emission intensities require an increased O_2 column density. The O column density must also increase to explain the excess 130.4-nm emissions, but since these include a contribution from solar resonance scattering, which is not dependent on T_e or n_e, the increase in O column density is relatively less than that for O_2. Hence, the O/O_2 mixing ratio required to produce the observed OI]

135.6-nm/ OI 130.4-nm intensity ratios on Ganymede's trailing hemisphere is reduced for small n_e and T_e. At $n_e = 70$ cm^{-3}, the electron density used in the Marconi (2007) models of Ganymede's atmosphere, the O/O$_2$ mixing ratio may be below 5% if the electron temperature is ~20 eV, and the O$_2$ column density is at the upper limit of previously derived ranges. However, this is likely an underestimate: electron density profiles derived by Eviatar, Vasyliūnas, et al. (2001) from the Galileo G1 and G2 flybys indicate that during both flybys n_e increased from ~100 cm^{-3} at 1.2 R$_G$, near the edge of the extraction region for our STIS spectra, to ~200 cm^{-3} at the closest approach of 1.1 R$_G$. They predict a surface density of ~400 cm^{-3}.

The dependence of the FUV oxygen emission on electron temperature and density make it difficult to fully constrain Ganymede's atmospheric composition in the absence of in situ plasma measurements. However, the models described here indicate that atomic oxygen comprises an important fraction of the trailing hemisphere atmosphere, potentially ~10–15% based on the electron temperatures implicated by Eviatar, Strobel, et al. (2001) and previous estimates of n_e.

A hemispheric difference in O/O$_2$ mixing ratio has also been observed at Europa: Roth et al. (2016) show that Europa's leading hemisphere FUV OI emissions are consistent with O/O$_2$ < 1% but require a ~5% O/O$_2$ mixing ratio on the trailing hemisphere, based on a mean OI emission ratio of 1.63 ± 0.05 and expected T_e of ~20 eV. They suggest that the hemispherical asymmetry at Europa may be due to lower T_e in the wake region, which would lead to a lower rate of dissociation of O$_2$ to O on the leading hemisphere. At Ganymede, this explanation appears less likely since the electrons responsible for the emissions are accelerated in the magnetosphere to temperatures much higher than the 10 eV expected in Europa's wake (Eviatar, Strobel, et al., 2001) and the decrease in the rate of dissociation of O$_2$ with electron temperature above the peak at $T_e \sim$ 30 eV is very gradual (Cosby, 1993).

The observed differences between Ganymede's leading and trailing hemisphere atmospheres may instead be related to previously observed surface dichotomies. Absorption features of O$_2$ and O$_3$ have been observed in reflectance spectra of the trailing hemisphere with no clear evidence of similar features on the leading hemisphere (Calvin et al., 1995; Nelson et al., 1987; Noll et al., 1996; Spencer et al., 1995). Hendrix et al. (1999) show that the strength of the trailing hemisphere O$_3$ absorption is strongly dependent on solar zenith angle and suggest that photodissociation of the ozone into O$_2$ and O occurs during the day. Hemispherical differences in oxygen chemistry such as this may contribute to the observed differences in the FUV oxygen emissions at Ganymede.

4.1.2. Application of the Atmosphere Model to the Auroral Regions

The atmospheric model derived above used disk-averaged auroral intensities for simplicity, but it is clear from Figure 2 that large areas of Ganymede are relatively dark at 135.6 and 130.4 nm. The disk-averaged calculation is therefore likely to underestimate the atmospheric density as brighter, localized emissions are modeled as dimmer, global emissions. In order to estimate the O and O$_2$ column densities required to produce the localized bright aurora we first produced histograms of the STIS 135.6 nm images and identified a threshold based on the approximately Gaussian distribution of pixel brightness above this value, which we attribute to discrete bright aurora, and the less defined distribution at lower intensities that we attribute to a background of dimmer, diffuse auroral emissions as described by previous authors (Eviatar, Strobel, et al., 2001; Feldman et al., 2000; McGrath et al., 2013). For the trailing hemisphere images this threshold was ~50 R. We then masked the 135.6-nm images to include only pixels with intensities greater than the threshold and masked the 130.4-nm images to include only pixels colocated with these bright 135.6-nm pixels. Examples of the STIS histogram and masked 135.6-nm image are shown in Figure 6a. From the masked images we derive mean auroral intensities of I(135.6 nm) = 74 ± 14 R and I(130.4 nm) = 46 ± 9 R on Ganymede's trailing hemisphere. This gives a 130.4-nm excess of 14 R over the expected emissions from dissociative excitation of O$_2$ based on the nominal OI] 135.6-nm/OI 130.4-nm ratio of 2.3.

Figures 6b and 6c show the O and O$_2$ column densities and O/O$_2$ ratios of model atmospheres that can produce the intensities measured in the masked auroral images for the same range of n_e and T_e used in the disk-averaged atmosphere model. The required column densities are slightly higher than those derived using the disk-averaged model and the corresponding O/O$_2$ ratios are slightly reduced, but an atomic oxygen mixing ratio of ~10% is still required for most electron densities with the 75- to 300-eV electron
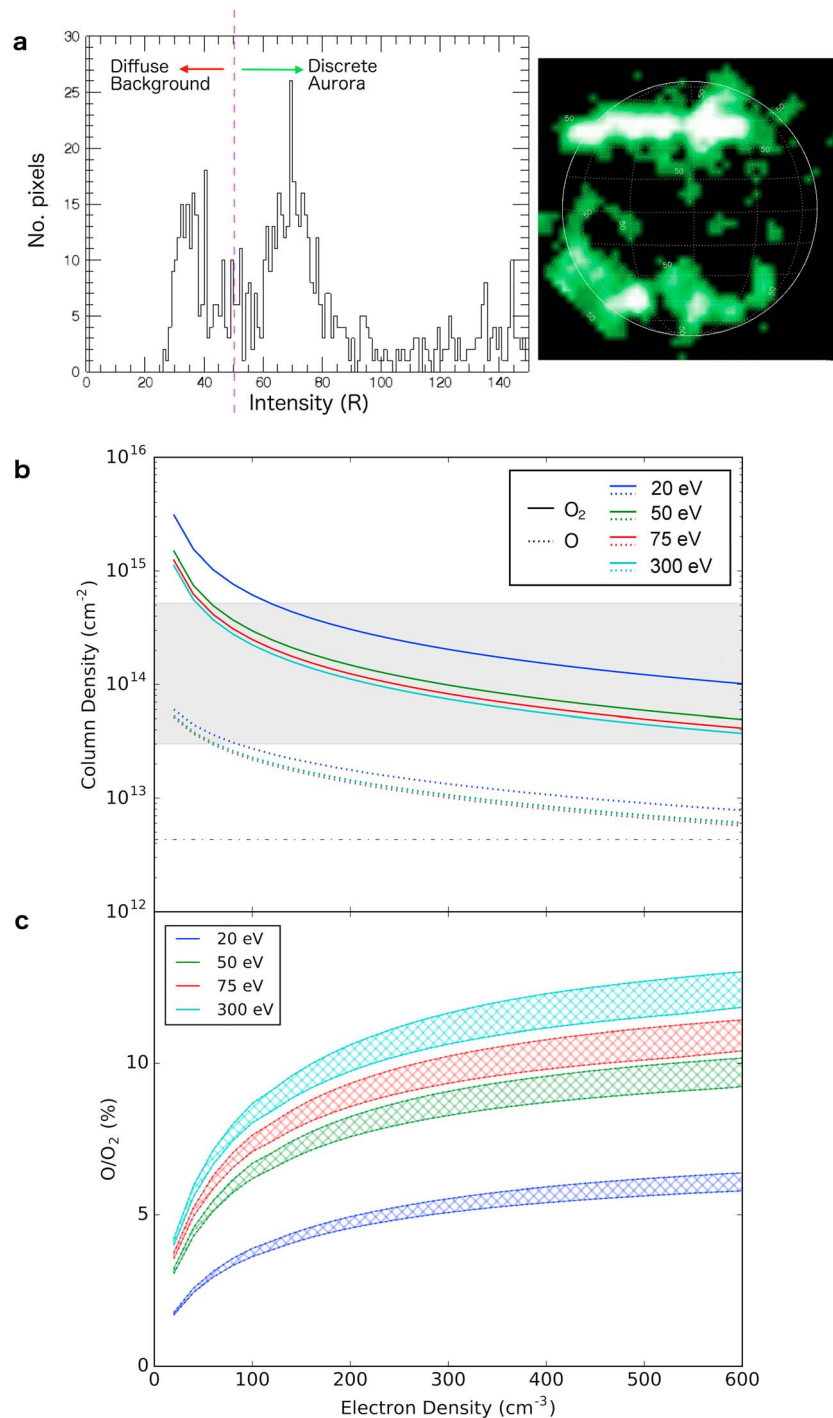
Figure 6. (a) Example of a Space Telescope Imaging Spectrograph 135.6-nm histogram, indicating the approximate threshold between diffuse background emissions and discrete aurora, alongside a 135.6-nm image of Ganymede's trailing hemisphere masked to include only pixels brighter than this threshold. (b) Column densities of O and O_2 required to produce the mean emissions in thresholded trailing hemisphere STIS images, similar to Figure 5a. (c) O/O_2 ratio derived from the column densities shown in (b) for an atmosphere that is optically thick at 130.4 nm, similar to Figure 5c.

temperatures derived by Eviatar, Strobel, et al. (2001). The O column densities we calculated using the auroral atmosphere model ranged from 5.7×10^{12} cm^{-2} for $n_e = 600$ cm^{-3} and $T_e = 75$ eV to 6.0×10^{13} cm^{-2} for $n_e = 20$ cm^{-3} and $T_e = 20$ eV. The O/O_2 ratio may be as low as 7% for $n_e = 100$ cm^{-3} if $T_e = 75$ eV, and the O_2 density is at the upper limit of the previously estimated range.

The brightest auroral emissions on Ganymede's trailing hemisphere reach intensities >200 R. This may be explained by localized regions of increased electron density and/or variations in electron temperature, but given the low number of images and the lack of in situ plasma measurements, we do not attempt to constrain this further.

4.1.3. STIS Color Ratio Images

Color ratio images derived from the 135.6- and 130.4-nm STIS images are shown in Figure 2. While these should be interpreted cautiously, as they were derived from data that had already been resampled and smoothed, we note that the trailing hemisphere images (Figures 2c and 2d) include large regions on Ganymede's disk where the 135.6-/130.4-nm color ratio is <1. This is consistent with the presence of solar resonance scattering by an atmosphere that is optically thick at 130.4 nm, as predicted by our models: for an optically thin atmosphere we would expect both 135.6- and 130.4-nm images to be dominated by noise away from the auroral regions, which would result in patchier color ratio images with no clear dominance of color ratios either greater than or less than unity.

4.2. Variations in the Brightness of Individual Multiplets

4.2.1. Brightness Variations Between Hemispheres

The brightness of the two OI multiplets varied between orbital hemispheres but also with λ_{III}. Our first and final sets of STIS observations (LS1 + LS2; TS3 + TS4) were obtained at similar λ_{III} (see Table 1) and therefore allow us to compare the auroral intensity on the two hemispheres directly with minimal λ_{III} influence. The 135.6-nm emissions were brighter on the leading hemisphere by a factor of ~1.5, with a mean intensity of 51 ± 8 R measured there, compared to 35 ± 4 R on the trailing hemisphere. The total 130.4-nm intensity was slightly higher on the trailing hemisphere (leading: 18 ± 7 R; trailing: 26 ± 7 R), but this included a contribution from resonance scattering and electron impact on O that is not observed on the leading hemisphere. After correcting for the mean trailing hemisphere 130.4-nm excess of 11 R (see section 4.1), the 130.4- and 135.6-nm emissions from dissociative excitation of O_2 are both brighter on the leading hemisphere. This proportional increase in the intensity of both emissions may be explained by a leading hemisphere electron density that is enhanced by a factor of 1.5 ± 0.4 relative to that on the trailing hemisphere or an O_2 atmosphere that is a factor of 1.5 ± 0.4 denser on the leading hemisphere. Recent models by Leblanc et al. (2017) show that the distribution of O_2 in Ganymede's atmosphere varies with orbital phase, with the largest column densities predicted on the sunlit (leading) hemisphere at a phase of 90°. Additionally, MHD models by Payan et al. (2015) indicate that the electron density is higher on the leading hemisphere. Consequently, the enhancement in the auroral brightness on the leading hemisphere may feasibly be related to increased $N[O_2]$, increased n_e, or a combination of the two. Finally, a variation in T_e between the two hemispheres may also contribute to the observed difference, but this is difficult to quantify without some initial constraint since there is not a linear relationship between electron temperature and emission cross section.

The observations of Ganymede's two hemispheres were obtained ~33 days apart, so there may also be a temporal component to the observed difference. However, brighter leading hemisphere auroral emissions are consistent with previous observations (McGrath et al., 2013; Musacchio et al., 2017) and with MHD models (Payan et al., 2015).

4.2.2. Brightness Changes Near the Plasma Sheet Crossings

We observed an increase in intensity in Ganymede's leading hemisphere aurora near the $\lambda_{III} = 291°$ plasma sheet crossing and a slight decrease in the trailing hemisphere intensity near the $\lambda_{III} = 111°$ crossing. Changes in intensity near the plasma sheet equator have been previously observed in the aurora of Ganymede (Musacchio et al., 2017), Europa (Roth et al., 2016; Saur et al., 2011) and Io (Oliversen et al., 2001; Retherford et al., 2000, Retherford et al., 2003; Roth et al., 2014; Wolven et al., 2001). At Io and Europa, both leading and trailing hemisphere emissions intensify, most probably due to the increased plasma density near the magnetic equator (e.g., Roth et al., 2014, 2016). At Ganymede, the interaction with the Jovian plasma is complicated by the presence of the moon's magnetosphere. Inside the plasma sheet, Ganymede's aurora moves to higher latitudes on the trailing hemisphere and lower latitudes on the leading side (Jia et al., 2008, 2009; McGrath et al., 2013). Musacchio et al. (2017) attribute the dimmer trailing hemisphere aurora to this shift, which corresponds to a larger fraction of the magnetospheric current closing in the downstream (leading) ionosphere. Additionally, the Alfvén Mach number (M_A) of the Jovian plasma may approach or even exceed 1 near the center of the plasma sheet at Ganymede's orbit (Paty et al., 2008; Paty & Winglee, 2004,

2006). If the upstream flow becomes super-Alfvénic ($M_A > 1$) an upstream shock will form, limiting the access of precipitating electrons to the flow-facing (trailing) hemisphere. Auroral brightness simulations based on these models predict that Ganymede's trailing hemisphere aurora will appear weaker when the satellite is within the Jovian plasma sheet for this reason (Payan et al., 2015).

5. Conclusions

We have analyzed the OI] 135.6-nm/OI 130.4-nm intensity ratio at Ganymede extracted from HST/STIS and HST/COS data and find a range of values that are best explained by a significant difference in the atmospheric compositions of the satellite's leading and trailing hemispheres. The mean ratio of 2.72 ± 0.57 observed on the leading hemisphere is consistent with an atmosphere comprising >99% O_2 but the observed trailing hemisphere ratio (1.42 ± 0.16) suggests that a substantial fraction of the atmosphere there comprises atomic oxygen. The O/O_2 mixing ratio required to explain the FUV emission ratio is dependent on the temperature and density of the electrons exciting the emissions. These parameters are not well constrained, but based on the 75–300 eV electron temperature derived by Eviatar, Strobel, et al. (2001) at Ganymede, the trailing hemisphere O/O_2 ratio is likely ~10%.

Our estimated O column density of 4.4×10^{12} to 6.0×10^{13} cm^{-2} on the trailing hemisphere suggests that the atmosphere is optically thick to the OI 130.4-nm radiation. An optically thin atmosphere could only produce the excess trailing hemisphere 130.4-nm emissions if the electron density is considerably higher than previous analyses have assumed, which would also imply that the O_2 column density has previously been overestimated. It is difficult to constrain n_e further without in situ measurements but the presence of an optically thick O atmosphere may be tested for in the future by observing the behavior of the 130.4-nm emissions as Ganymede moves into eclipse: if the atmosphere is optically thick then the 130.4-nm emissions will be reduced during eclipse in the absence of solar resonance scattering. Alternatively, observations at higher spectral resolution could be used to determine the ratio of the individual spectral components within the 130.4-nm multiplet. If the atmosphere is optically thin, the ratio of the emission intensities should be equal to the ratio of their transition probabilities. The O_2 abundance may be constrained through stellar occultation observations near the auroral regions: O_2 has several strong absorption bands, for example, the Schumann-Runge continuum around 135–176 nm, which may be observed in the spectra of stars as they are occulted by Ganymede, and the observed magnitude of the absorption used to constrain the atmospheric O_2 density.

When comparing observations of the leading and trailing hemispheres at similar System III longitudes, we find that the auroral emissions due to dissociative excitation of O_2 are enhanced on the leading hemisphere. This may be due to an enhancement of 1.5 ± 0.4 in either $N[O_2]$ or n_e on the leading hemisphere relative to the trailing, or to variations in both parameters simultaneously. Hemispheric differences in T_e may also contribute to different auroral intensities. The mean auroral intensity was also higher on the leading hemisphere, and the standard deviation was larger there, indicating more variation in the leading hemisphere aurora than in the trailing hemisphere aurora during this observation campaign.

Finally, we observe a difference in the response of the leading and trailing hemisphere aurora when Ganymede moves close to the plasma sheet equator, with an increase in the emission intensity seen on the leading hemisphere and a reduction in the brightness of the trailing hemisphere emissions. This has previously been attributed to an observed shift in the location of the aurora to higher latitudes on the trailing hemisphere and lower latitudes on the leading hemisphere (Musacchio et al., 2017). However, a larger Alfvén Mach number due to the increased plasma density and weaker Jovian magnetic field near the magnetic equator is predicted to produce a similar effect by reducing the access of electrons to the trailing hemisphere.

References

Bagenal, F., Sidrow, E., Wilson, R. J., Cassidy, T. A., Dols, V., Crary, F., et al. (2015). Plasma conditions at Europa's orbit. *Icarus*, *261*, 1–13. https://doi.org/10.1016/j.icarus.2015.07.036

Barth, C. A. (1969). Planetary ultraviolet spectroscopy. *Applied Optics*, *8*(7), 1295–1304. https://doi.org/10.1364/AO.8.001295

Broadfoot, A. L., Sandel, B. R., Shemansky, D. E., McConnell, J. C., Smith, G. R., Holberg, J. B., et al. (1981). Overview of Voyager ultraviolet spectrometry results through Jupiter encounter. *Journal of Geophysical Research*, *86*, 8259–8284. https://doi.org/10.1029/JA086iA10p08259

Calvin, W. M., Clark, R. N., Brown, R. H., & Spencer, J. R. (1995). Spectra of the icy Galilean satellites from 0.2 to 5 μm: A compilation, new observations, and a recent summary. *Journal of Geophysical Research*, *100*, 19,041–19,048. https://doi.org/10.1029/94JE03349

Connerney, J. E. P., Acuna, M. H., Ness, N. F., & Satoh, T. (1998). New models of Jupiter's magnetic field constrained by the Io flux tube footprint. *Journal of Geophysical Research*, *103*, 11,929–11,939. https://doi.org/10.1029/97JA03726

Cosby, P. C. (1993). Electron-impact dissociation of oxygen. *Journal of Chemical Physics*, *98*(12), 9560–9569. https://doi.org/10.1063/1.464387

Cotton, D. M., Chakrabarti, S., & Gladstone, G. R. (1993). Optically thick cascade to the O I 3s ^{3}S state in the Earth's thermosphere. *Journal of Geophysical Research*, *98*, 21,643–21,650. https://doi.org/10.1029/93JA02266

Duling, S., Saur, J., & Wicht, J. (2014). Consistent boundary conditions at nonconducting surfaces of planetary bodies: Applications in a new Ganymede MHD model. *Journal of Geophysical Research: Space Physics*, *119*, 4412–4440. https://doi.org/10.1002/2013JA019554

Eviatar, A., Strobel, D. F., Wolven, B. C., Feldman, P. D., McGrath, M. A., & Williams, D. J. (2001). Excitation of the Ganymede ultraviolet aurora. *Astrophysical Journal*, *555*(2), 1013–1019. https://doi.org/10.1086/321510

Eviatar, A., Vasyliūnas, V. M., & Gurnett, D. A. (2001). The ionosphere of Ganymede. *Planetary and Space Science*, *49*(3-4), 327–336. https://doi.org/10.1016/S0032-0633(00)00154-9

Feldman, P. D., McGrath, M. A., Strobel, D. F., Moos, H. W., Retherford, K. D., & Wolven, B. C. (2000). HST/STIS ultraviolet imaging of polar aurora on Ganymede. *Astrophysical Journal*, *535*(2), 1085–1090. https://doi.org/10.1086/308889

Green, J. C., Froning, C. S., Osterman, S., Ebbets, D., Heap, S. H., Leitherer, C., et al. (2012). The Cosmic Origins Spectrograph. *Astrophysical Journal*, *744*(1), 60. https://doi.org/10.1088/0004-637X/744/1/60

Gurnett, D. A., Kurth, W. S., Roux, A., Bolton, S. J., & Kennel, C. F. (1996). Evidence for a magnetosphere at Ganymede from plasma-wave observations by the Galileo spacecraft. *Nature*, *384*(6609), 535–537. https://doi.org/10.1038/384535a0

Hall, D. T., Feldman, P. D., McGrath, M. A., & Strobel, D. F. (1998). The far-ultraviolet oxygen airglow of Europa and Ganymede. *Astrophysical Journal*, *499*(1), 475–481. https://doi.org/10.1086/305604

Hall, D. T., Stobel, D. F., Feldman, P. D., McGrath, M. A., & Weaver, H. A. (1995). Detection of an oxygen atmosphere on Jupiter's moon Europa. *Nature*, *373*(6516), 677–679. https://doi.org/10.1038/373677a0

Hendrix, A. R., Barth, C. A., & Hord, C. W. (1999). Ganymede's ozone-like absorber: Observations by the Galileo ultraviolet spectrometer. *Journal of Geophysical Research*, *104*, 14,169–14,178. https://doi.org/10.1029/1999JE900001

Hess, S. L. G., Bonfond, B., Zarka, P., & Grodent, D. (2011). Model of the Jovian magnetic field topology constrained by the Io auroral emissions. *Journal of Geophysical Research*, *116*, A05217. https://doi.org/10.1029/2010JA016262

Jia, X., Walker, R. J. K., Kivelson, M. G., Khurana, K., & Linker, J. A. (2009). Properties of Ganymede's magnetosphere inferred from improved three-dimensional MHD simulations. *Journal of Geophysical Research*, *114*, A09209. https://doi.org/10.1029/2009JA014375

Jia, X., Walker, R. J., Kivelson, M. G., Khurana, K. K., & Linker, J. A. (2008). Three-dimensional MHD simulations of Ganymede's magnetosphere. *Journal of Geophysical Research*, *113*, A06212. https://doi.org/10.1029/2007JA012748

Kanik, I., Noren, C., Makarov, O. P., Vattipalle, P., Ajello, J. M., & Shemansky, D. E. (2003). Electron impact dissociative excitation of O2: 2. Absolute emission and cross sections of the OI(130.4 nm) and OI(135.6 nm) lines. *Journal of Geophysical Research*, *108*(E11), 5126. https://doi.org/10.1029/2000JE001423

Kivelson, M. G., Khurana, K. K., Coroniti, F. V., Joy, S., Russell, C. T., Walker, R. J., et al. (1997). The magnetic field and magnetosphere of Ganymede. *Geophysical Research Letters*, *24*, 2155–2158. https://doi.org/10.1029/97GL02201

Kivelson, M. G., Khurana, K. K., Russell, C. T., Walker, R. J., Warnecke, J., Coroniti, F. V., et al. (1996). Discovery of Ganymede's magnetic field by the Galileo spacecraft. *Nature*, *384*(6609), 537–541. https://doi.org/10.1038/384537a0

Koga, R., Tsuchiya, F., Kagitani, M., Sakanoi, T., Yoneda, M., Yoshioka, K., et al. (2018). The time variation of atomic oxygen emission around Io during a volcanic event observed with Hisaki/EXCEED. *Icarus*, *299*, 300–307. https://doi.org/10.1016/j.icarus.2017.07.024

Laher, R. R., & Gilmore, F. R. (1990). Updated excitation and ionization cross sections for electron impact on atomic oxygen. *Journal of Physical and Chemical Reference Data*, *19*(1), 277–305. https://doi.org/10.1063/1.555872

Leblanc, F., Oza, A. V., Leclercq, L., Schmidt, C., Cassidy, T., Modolo, R., et al. (2017). On the orbital variability of Ganymede's atmosphere. *Icarus*, *293*, 185–198. https://doi.org/10.1016/j.icarus.2017.04.025

Lee, J.-S., & Meier, R. R. (1980). Angle-dependent frequency redistribution in a plane-parallel medium: External source case. *Astrophysical Journal*, *240*, 185. https://doi.org/10.1086/158222

Marconi, M. L. (2007). A kinetic model of Ganymede's atmosphere. *Icarus*, *190*(1), 155–174. https://doi.org/10.1016/j.icarus.2007.02.016

McGrath, M. A., Jia, X., Retherford, K. D., Feldman, P. D., Strobel, D. F., & Saur, J. (2013). Aurora on Ganymede. *Journal of Geophysical Research: Space Physics*, *118*, 2043–2054. https://doi.org/10.1002/jgra.50122

Musacchio, F., Saur, J., Roth, L., Retherford, K. D., McGrath, M. A., Feldman, P. D., & Strobel, D. F. (2017). Morphology of Ganymede's FUV auroral ovals. *Journal of Geophysical Research*, *122*, 2855–2876. https://doi.org/10.1002/2016JA023220

Nelson, R. M., Lane, A. L., Matson, D. L., Veeder, G. J., Buratti, B. J., & Tedesco, E. F. (1987). Spectral geometric albedos of the Galilean satellites from 0.24 to 0.34 micrometers: Observations with the international ultraviolet explorer. *Icarus*, *72*(2), 358–380. https://doi.org/10.1016/0019-1035(87)90180-1

Noll, K. S., Johnson, R. E., Lane, A. L., Domingue, D. L., & Weaver, H. A. (1996). Detection of ozone on Ganymede. *Science*, *273*(5273), 341–343. https://doi.org/10.1126/science.273.5273.341

Oliversen, R. J., Scherb, F. W., Smyth, H., Freed, M. E., Woodward, R. C. Jr., Marconi, M. L., et al. (2001). Sunlit Io atmosphere [O I] 6300 Å emission and the plasma torus. *Journal of Geophysical Research*, *106*, 26,183–26,193. https://doi.org/10.1029/2000JA002507

Paty, C., Paterson, W., & Winglee, R. (2008). Ion energization in Ganymede's magnetosphere: Using multifluid simulations to interpret ion energy spectrograms. *Journal of Geophysical Research*, *113*, A06211. https://doi.org/10.1029/JA012848

Paty, C., & Winglee, R. (2004). Multi-fluid simulations of Ganymede's magnetosphere. *Geophysical Research Letters*, *31*, L24806. https://doi.org/10.1029/2004GL021220

Paty, C., & Winglee, R. (2006). The role of ion cyclotron motion at Ganymede: Magnetic field morphology and magnetospheric dynamics. *Geophysical Research Letters*, *33*, L10106. https://doi.org/10.1029/2005GL025273

Payan, A. P., Paty, C. S., & Retherford, K. D. (2015). Uncovering local magnetospheric processes governing the morphology and variability of Ganymede's aurora using three-dimensional multifluid simulations of Ganymede's magnetosphere. *Journal of Geophysical Research: Space Physics*, *120*, 401–413. https://doi.org/10.1002/2014JA020301

Retherford, K. D., Moos, H. W., & Strobel, D. F. (2003). Io's auroral limb glow: Hubble Space Telescope FUV observations. *Journal of Geophysical Research*, *108*(A8), 1333. https://doi.org/10.1029/2002JA009710

Retherford, K. D., Moos, H. W., Strobel, D. F., & Wolven, B. C. (2000). Io's equatorial spots: Morphology of neutral UV emissions. *Journal of Geophysical Research*, *105*, 27,157–27,165. https://doi.org/10.1029/2000JA002500

Roth, L., Saur, J., Retherford, K. D., Strobel, D. F., & Feldman, P. D. (2014). A phenomenological model of Io's UV aurora based on HST/STIS observations. *Icarus*, *228*, 386–406. https://doi.org/10.1016/j.icarus.2013.10.009

Roth, L., Saur, J., Retherford, K. D., Strobel, D. F., Feldman, P. D., McGrath, M. A., et al. (2016). Europa's far-ultraviolet oxygen aurora from a comprehensive set of HST observations. *Journal of Geophysical Research: Space Physics*, *121*, 2143–2170. https://doi.org/10.1002/2015JA022073

Saur, J., Duling, S., Roth, L., Jia, X., Strobel, D. F., Feldman, P. D., et al. (2015). The search for a subsurface ocean in Ganymede with Hubble Space Telescope observations of its auroral ovals. *Journal of Geophysical Research: Space Physics*, *120*, 1715–1737. https://doi.org/10.1002/2014JA020778

Saur, J., Feldman, P. D., Roth, L., Nimmo, F., Strobel, D. F., Retherford, K. D., et al. (2011). Hubble Space Telescope/ Advanced Camera for Surveys observations of Europa's atmospheric ultraviolet emission at eastern elongation. *Astrophysical Journal*, *738*(2), 153. https://doi.org/10.1088/0004-637X/738/2/153

Spencer, J. R., Calvin, W. M., & Person, M. J. (1995). Charge-coupled device spectra of the Galilean satellites: Molecular oxygen on Ganymede. *Journal of Geophysical Research*, *100*, 19,049–19,056. https://doi.org/10.1029/95JE01503

Stone, E. J., & Zipf, E. C. (1974). Electron-impact excitation of the $^3S^0$ and $^5S^0$ states of atomic oxygen. *Journal of Chemical Physics*, *60*(11), 4237–4243. https://doi.org/10.1063/1.1680894

Wolven, B. C., Moos, H. W., Retherford, K. D., Feldman, P. D., Strobel, D. F., Smyth, W. H., & Roesler, F. L. (2001). Emission profiles of neutral oxygen and sulfur in Io's exospheric corona. *Journal of Geophysical Research*, *106*, 26,155–26,182. https://doi.org/10.1029/2000JA002506

Woods, T. N., Bailey, S., Eparvier, F., Lawrence, G., Lean, J., et al. (2000). TIMED Solar EUV experiment. *Physics and Chemistry of the Earth, Part C: Solar, Terrestrial and Planetary Science*, *25*(5-6), 393–396. https://doi.org/10.1016/S1464-1917(00)00040-4